Predicting ocean pressure field with a physics-informed neural network

使用物理信息神经网络预测海洋压力场

Seunghyun Yoon, [1,2] Yongsung Park, [2,a] Depeter Gerstoft, [2] D and Woojae Seong [1,3] D

Seunghyun Yoon, [1,2] Yongsung Park, [2,a] Depeter Gerstoft, [2] D 和 Woojae Seong [1,3] D

[1] Department of Naval Architecture and Ocean Engineering, Seoul National University, Seoul 08826, Republic of Korea

[1] 韩国首尔国立大学海洋工程系，首尔 08826

[2] Scripps Institution of Oceanography, University of California San Diego, La Jolla, California 92093-0238, USA

[2] 美国加利福尼亚大学圣地亚哥分校斯克里普斯海洋研究所，拉霍亚，加利福尼亚 92093 - 0238

[3] Research Institute of Marine Systems Engineering, Seoul National University, Seoul 08826, Republic of Korea

[3] 韩国首尔国立大学海洋系统工程研究所，首尔 08826

ABSTRACT:

摘要:

Ocean sound pressure field prediction, based on partially measured pressure magnitudes at different range-depths, is presented. Our proposed machine learning strategy employs a trained neural network with range-depth as input and outputs complex acoustic pressure at the location. We utilize a physics-informed neural network (PINN), fitting sampled data while considering the additional information provided by the partial differential equation (PDE) governing the ocean sound pressure field. In vast ocean environments with kilometer-scale ranges, pressure fields exhibit rapidly fluctuating phases, even at frequencies below 100 Hz , posing a challenge for neural networks to converge to accurate solutions. To address this, we utilize the envelope function from the parabolic-equation technique, fundamental in ocean sound propagation modeling. The envelope function shows slower variations across ranges, enabling PINNs to predict sound pressure in an ocean waveguide more effectively. Additional PDE information allows PINNs to capture PDE solutions even with a limited amount of training data, distinguishing them from purely data-driven machine learning approaches that require extensive datasets. Our approach is validated through simulations and using data from the SWellEx-96 experiment.

本文提出了基于不同距离 - 深度处部分测量压力幅值的海洋声压场预测方法。我们提出的机器学习策略采用经过训练的神经网络，以距离 - 深度作为输入，并输出该位置的复声压。我们利用物理信息神经网络 (PINN)，在拟合采样数据的同时考虑由控制海洋声压场的偏微分方程 (PDE) 提供的额外信息。在千米级距离的广阔海洋环境中，即使在低于 100 Hz 的频率下，压力场也呈现出快速波动的相位，这给神经网络收敛到精确解带来了挑战。为了解决这个问题，我们利用抛物方程技术中的包络函数，它在海洋声传播建模中至关重要。包络函数在距离上的变化较慢，使 PINN 能够更有效地预测海洋波导中的声压。额外的 PDE 信息使 PINN 即使在训练数据有限的情况下也能捕捉 PDE 解，这使其有别于需要大量数据集的纯数据驱动机器学习方法。我们的方法通过模拟和使用 SWellEx - 96 实验的数据进行了验证。©2024 美国声学学会。

https://doi.org/10.1121/10.0025235

(Received 24 June 2023; revised 19 February 2024; accepted 21 February 2024; published online 13 March 2024) [Editor: Zoi-Heleni Michalopoulou] Pages: 2037-2049

(2023 年 6 月 24 日收到；2024 年 2 月 19 日修订；2024 年 2 月 21 日接受；2024 年 3 月 13 日在线发表) [编辑:Zoi - Heleni Michalopoulou] 页码:2037 - 2049

I. INTRODUCTION

一、引言

Sound propagation in the ocean has representations governed by physical laws in ocean acoustic environments. A physics-informed neural network (PINN) [1] trains the neural network using sampled data and encodes the underlying physical laws governing the dataset, represented with partial differential equations (PDEs). We present a PINN-based strategy that offers a realistic prediction of ocean acoustic propagation.

海洋中的声传播由海洋声学环境中的物理定律描述。物理信息神经网络 (PINN) [1] 使用采样数据训练神经网络，并对由偏微分方程 (PDE) 表示的控制数据集的基础物理定律进行编码。我们提出了一种基于 PINN 的策略，可对海洋声传播进行实际预测。

In this study, we present OceanPINN, a machine learning framework for predicting ocean acoustic pressure fields. A PINN is fitted to the partially observed experimental data while integrating prior scientific knowledge. OceanPINN utilizes pressure magnitude data from various range-depths for data fitting. Beyond fitting data at known points, OceanPINN enforces the underlying physics of the ocean waveguide, including governing partial differential equation (PDE) and the pressure-release surface boundary condition, which enables extended predictions to unknown points. A sound speed profile (SSP) is required as prior information to compute the governing PDE. Once trained, the OceanPINN can predict the sound pressure field at any given range-depth. The predicted pressure field has a wide range of applications, such as source localization, [2–4] sonar performance assessment, [5,6] and noise prediction for marine mammals. [7,8]

在本研究中，我们提出了 OceanPINN——一种用于预测海洋声压场的机器学习框架。将 PINN 拟合到部分观测的实验数据上，同时整合先验科学知识。OceanPINN 利用来自不同距离 - 深度的压力幅值数据进行数据拟合。除了在已知点拟合数据外，OceanPINN 还强化了海洋波导的基础物理，包括控制偏微分方程 (PDE) 和压力释放表面边界条件，这使得能够对未知点进行扩展预测。需要声速剖面 (SSP) 作为先验信息来计算控制 PDE。一旦训练完成，OceanPINN 可以预测任何给定距离 - 深度处的声压场。预测的压力场有广泛的应用，如源定位、[2–4] 声纳性能评估、[5,6] 以及海洋哺乳动物的噪声预测。[7,8]

Many papers have adopted machine learning methods for ocean acoustics problems through purely data-driven approaches. [9–19] A few studies have explored integrating physical knowledge into neural networks by applying PINN to estimate modal wavenumbers [20] or by modifying the machine learning framework to satisfy a ray or modal solution. [21,22] Recently, PINN has been applied for underwater pressure prediction. [23] However, the research has focused on an ideal environment with small domain sizes and simple environmental conditions. Our objective is to enable a PINN framework that works in more realistic ocean acoustic environments with kilometer-scale ranges.

许多论文通过纯数据驱动的方法将机器学习方法应用于海洋声学问题。[9–19] 一些研究探索了通过应用 PINN 估计模态波数将物理知识整合到神经网络中，[20] 或者通过修改机器学习框架以满足射线或模态解。[21,22] 最近，PINN 已应用于水下压力预测。[23] 然而，研究主要集中在小区域尺寸和简单环境条件的理想环境中。我们的目标是实现一个能在千米级距离的更实际海洋声学环境中工作的 PINN 框架。

Purely data-driven machine learning approaches require extensive training datasets to learn the PDE solutions. In contrast, the PINN-based method encourages the network to learn the structural information expressed by the PDEs, facilitating the network to capture the PDE solutions well, even with a low amount of training data.

纯数据驱动的机器学习方法需要大量的训练数据集来学习 PDE 解。相比之下，基于 PINN 的方法鼓励网络学习由 PDE 表达的结构信息，即使训练数据量少，也有助于网络很好地捕捉 PDE 解。

PINN has been applied to various fields, including seismology, [24] fluid dynamics, [25] and biophysics. [26] In various acoustic field predictions, PINNs have been employed to solve the Helmholtz [27–29] or wave equation. [30,31] However, these applications involve smaller domain sizes [23,31] or lower frequencies, [27–30] resulting in less complex fields compared to our focus on kilometer-scale real ocean acoustic fields.

PINN 已应用于多个领域，包括地震学、[24] 流体动力学、[25] 和生物物理学。[26] 在各种声场预测中，PINN 已被用于求解亥姆霍兹 [27–29] 或波动方程。[30,31] 然而，这些应用涉及的区域尺寸较小 [23,31] 或频率较低，[27–30] 与我们关注的千米级真实海洋声场相比，其场的复杂性较低。

Despite the success of PINNs, recent studies [32,33] have shown their limitations in complex PDE problems. Specifically, fully connected neural networks, commonly used in the architecture of PINNs, suffer from a fundamental issue, known as spectral bias. [34] Spectral bias refers to the difficulty in learning high-frequency functions. The spectral bias problem in PINNs [32] was analyzed through neural tangent kernel theory, [35] revealing challenges in learning high-frequency functions. [36] Consequently, applying PINNs to a realistic ocean acoustics environment presents greater challenges due to spectral bias. In our approach, to address this spec-

tral bias, we transform the pressure field into a low-fluctuating representation, called an envelope. OceanPINN is trained to approximate this envelope, with the loss function incorporating the modified Helmholtz equation and pressure-release surface boundary conditions.

尽管 PINNs 取得了成功，但最近的研究 [32,33] 表明它们在复杂的偏微分方程问题中存在局限性。具体而言，PINNs 架构中常用的全连接神经网络存在一个基本问题，即频谱偏差。[34] 频谱偏差是指学习高频函数的困难。通过神经切线核理论 [32] 分析了 PINNs 中的频谱偏差问题，[35] 揭示了学习高频函数的挑战。[36] 因此，由于频谱偏差，将 PINNs 应用于实际海洋声学环境面临更大的挑战。在我们的方法中，为了解决这种频谱偏差，我们将压力场转换为一种低波动表示，称为包络。OceanPINN 经过训练以逼近这种包络，损失函数纳入了修正的亥姆霍兹方程和压力释放表面边界条件。

---

a)Email: yongsungpark@ucsd.edu

a) 电子邮件:yongsungpark@ucsd.edu

Ocean waveguides are typically modeled with two boundary conditions: a pressure-release ocean surface and a bottom with sediment layers. The propagation of acoustic waves within these waveguides is governed by the acoustic wave equation or the Helmholtz equation in the frequency domain. Conventionally, the governing equation is solved using ray theory, normal mode theory, and a parabolic equation model in the ocean environment. [37] The accuracy of acoustic wave field simulations is highly dependent on environmental parameters, including the SSP, bathymetry, and sediment properties. However, the vastness of the ocean can lead to situations with unknown environmental parameters. Direct measurement of sediment properties is challenging and is typically inferred through geoacoustic inversion methods [38–40] from measured acoustic signals. These inversion methods approximate the actual bottom using geoa-coustic models, requiring a certain degree of prior knowledge about the bottom in the area of interest. [41,42] The absence of this knowledge can substantially increase the range and number of model parameters needed for analysis. Furthermore, incorrect assumptions about the bottom model can lead to errors in the predicted fields. In contrast, OceanPINN does not require any prior knowledge of the bottom, distinguishing it from conventional model-based geoacoustic inversion methods.

海洋波导通常用两种边界条件建模: 压力释放海洋表面和有沉积层的底部。这些波导内声波的传播由频域中的声波方程或亥姆霍兹方程控制。传统上，在海洋环境中使用射线理论、简正模理论和抛物方程模型来求解控制方程。[37] 声波场模拟的准确性高度依赖于环境参数，包括声速剖面、地形和沉积物特性。然而，海洋的广阔性可能导致环境参数未知的情况。沉积物特性的直接测量具有挑战性，通常通过地球声学反演方法 [38–40] 从测量的声学信号中推断。这些反演方法使用地球声学模型近似实际底部，需要对感兴趣区域的底部有一定程度的先验知识。[41,42] 缺乏这些知识会大幅增加分析所需的模型参数范围和数量。此外，对底部模型的错误假设可能导致预测场中的误差。相比之下，OceanPINN 不需要关于底部的任何先验知识，这使其与基于传统模型的地球声学反演方法不同。

Working with ocean acoustic experimental data presents several challenges. First, array sizes are insufficient to cover the whole ocean waveguide. Additionally, due to the ocean's temporal variability, remeasuring in previously unmeasured areas is complicated, as environmental changes can alter data characteristics.

Moreover, accurately measuring the phase in experiments is challenging because of its sensitivity; the phase of ocean acoustic pressure is affected by the Doppler effect [43,44] and varies rapidly across the range. This sensitivity makes range-coherent processing difficult. OceanPINN can address these challenges by predicting unmeasured pressure fields with magnitude data and reconstructing phase information.

处理海洋声学实验数据存在几个挑战。首先，阵列尺寸不足以覆盖整个海洋波导。此外，由于海洋的时间变异性，在以前未测量的区域重新测量很复杂，因为环境变化会改变数据特征。而且，由于其敏感性，在实验中准确测量相位具有挑战性；海洋声压的相位受多普勒效应 [43,44] 影响，并且在整个范围内变化迅速。这种敏感性使得距离相干处理困难。OceanPINN 可以通过利用幅度数据预测未测量的压力场并重建相位信息来应对这些挑战。

In summary, we mitigate the spectral bias in PINNs using the low-fluctuating nature of the envelope that constructs acoustic pressure fields and this enables ocean acoustic pressure field prediction. OceanPINN does not require complex bottom modeling. Additionally, training OceanPINN with magnitude data enables the reconstruction of phase information, allowing for potential range-coherent processing and improving performance. OceanPINN is evaluated in simulation and experiment conducted in the shallow water evaluation cell experiment 1996 (SWellEx-96). [45,46]

总之，我们利用构建声压场的包络的低波动特性减轻了 PINN 中的频谱偏差，这使得海洋声压场预测成为可能。OceanPINN 不需要复杂的底部建模。此外，用幅度数据训练 OceanPINN 能够重建相位信息，允许进行潜在的距离相干处理并提高性能。在 1996 年浅水评估单元实验 (SWellEx - 96) 中进行的模拟和实验中对 OceanPINN 进行了评估。[45,46]

II. PINN-BASED PRESSURE FIELD PREDICTION

II. 基于 PINN 的压力场预测

In this section, we provide the required background and description of the proposed method. Section II A introduces the governing PDE and discusses the challenges of applying PINN in the ocean waveguide. Section II B explains the data preprocessing method to overcome these challenges. Section II C introduces the general PINN framework, and the proposed PINN-based ocean acoustic pressure field prediction method is described in Sec. II D.

在本节中，我们提供了所提出方法所需的背景和描述。第二部分 A 介绍了控制偏微分方程，并讨论了在海洋波导中应用 PINN 的挑战。第二部分 B 解释了克服这些挑战的数据预处理方法。第二部分 C 介绍了一般的 PINN 框架，基于 PINN 的海洋声压场预测方法在第二部分 D 中描述。

A. Pressure field in the ocean waveguide

A. 海洋波导中的压力场

The acoustic pressure field satisfies the Helmholtz equation. In an ocean waveguide with a constant-density medium and an azimuth-independent environment, the Helmholtz equation in range-depth coordinates (r, z) is expressed as [37]

声压场满足亥姆霍兹方程。在具有恒定密度介质和与方位无关环境的海洋波导中，距离 - 深度坐标下的亥姆霍兹方程 (r,z) 表示为 [37]

$$\frac{1}{r}\frac{\partial}{\partial r}\left(r\frac{\partial p}{\partial r}\right)+\frac{\partial^2 p}{\partial z^2}+\frac{\omega^2}{c^2}p=0, \tag{1}$$

where ω is an angular frequency, p is a pressure field, and c is a sound speed of medium. The notation (r,z) is abbreviated for variables p and c . The pressure field is obtained by solving the Helmholtz equation with boundary conditions.

其中 ω 是角频率，p 是压力场，c 是介质中的声速。符号 (r,z) 是变量 p 和 c 的缩写。压力场通过求解具有边界条件的亥姆霍兹方程获得。

Here, we detail the characteristics of the pressure field within an ocean waveguide. For simplicity, a range-independent environment is assumed. Consider a scenario in which a point source is at position (r,z_s) and a single receiver is at position $(0,z)$. The Helmholtz equation is solved with normal mode theory, [37] and the pressure field is a sum of normal modes as

在此，我们详细阐述海洋波导内压力场的特性。为简单起见，假设环境与距离无关。考虑一种情况，即点源位于 (r,z_s) 位置，单个接收器位于 $(0,z)$ 位置。利用简正波理论求解亥姆霍兹方程，[37] 且压力场是简正波的叠加，形式如下

$$p(r,z)=\frac{i}{4\rho(z_s)}\sum_{m=1}^{M}\Psi_m(z_s)\Psi_m(z)H_0^{(2)}(k_m r), \tag{2}$$

where k_m is the m th mode wavenumber, M is the number of propagating modes, and $\Psi_m(z)$ denotes the m th modal depth function. We adopt the second kind Hankel function $H_0^{(2)}(k_m r)$, as we use the Fourier transform pair in the time-frequency (t,f) domain as

其中 k_m 是第 m 阶模式波数，M 是传播模式的数量，并且 $\Psi_m(z)$ 表示第 m 阶模态深度函数。我们采用第二类汉克尔函数 $H_0^{(2)}(k_m r)$ ，因为我们在时频 (t,f) 域中使用傅里叶变换对作为

(3)

$$p(f)=\int_{-\infty}^{\infty}p(t)e^{-i2\pi ft}dt$$

$$p(t)=\int_{-\infty}^{\infty}p(f)e^{i2\pi ft}df$$

where the sign of the phase in the exponent term is opposite to Ref. 37. Mode wavenumbers are determined by environmental parameters (e.g., SSP and geoacoustic parameters).

指数项中相位的符号与参考文献 37 相反。模式波数由环境参数 (例如，声速剖面和地声参数) 确定。

We can compute the mode wavenumber in the perfectly known environment and generate the pressure field.

我们可以在完全已知的环境中计算模式波数并生成压力场。

Hankel function $H_0^{(2)}(k_m r)$ determines the pressure variation in range direction as Eq. (2). In the far field ($kr \gg 1$) , the Hankel function form is asymptotic,

汉克尔函数 $H_0^{(2)}(k_m r)$ 如式 (2) 所示确定距离方向上的压力变化。在远场 ($kr \gg 1$) 中，汉克尔函数形式是渐近的，

$$H_0^{(2)}(kr) \approx \sqrt{\frac{2}{\pi kr}} e^{-i(kr-\pi/4)}. \tag{4}$$

The phase of the Hankel function changes rapidly with slight range variations, causing the pressure field to exhibit rapid variations with respect to range. In contrast, the magnitude of the Hankel function, i.e., $\sqrt{2/\pi kr}$ changes slowly with respect to range. In Fig. 1, we present an example of a simulated pressure field using the Kraken normal mode model [47] in an isovelocity environment (see Sec. IV A for detail). As seen in Figs. 1(c) and 1(e), the real and imaginary component of the pressure field exhibits rapid variation with respect to range, while the magnitude changes gradually, as shown in Fig. 1(a). This characteristic of complex pressures presents two challenges: (1) The highly fluctuating patterns make training neural networks challenging. (2) Even a small error in range, denoted as Δr , results in a significant difference between the measured pressures $p(r,z)$ and $p(r+\Delta r,z)$. We can mitigate the second challenge by using the magnitude of measured pressure $|p|$ with lower sensitivity. The approach to address the first challenge is detailed in the subsequent section.

汉克尔函数的相位随范围的微小变化而迅速变化，导致压力场随范围呈现快速变化。相比之下，汉克尔函数的幅度，即 $\sqrt{2/\pi kr}$ 随范围变化缓慢。在图 1 中，我们给出了一个在等速环境中使用克拉肯简正波模型 [47] 模拟压力场的示例 (详细内容见第四节 A)。如图 1(c) 和 1(e) 所示，压力场的实部和虚部随范围呈现快速变化，而幅度则逐渐变化，如图 1(a) 所示。复压力的这一特性带来了两个挑战:(1) 高度波动的模式使训练神经网络具有挑战性。(2) 即使范围上有一个小误差，记为 Δr ，也会导致测量压力 $p(r,z)$ 和 $p(r+\Delta r,z)$ 之间存在显著差异。我们可以通过使用灵敏度较低的测量压力 $|p|$ 的幅度来减轻第二个挑战。解决第一个挑战的方法将在后续章节中详细介绍。

B. Smoothing the pressure field

B. 平滑压力场

To address the first challenge, we adopt an envelope $\psi(r,z)$ used in the derivation of the parabolic equation, [37]

为应对第一个挑战，我们采用了在抛物方程推导中使用的一个包络 $\psi(r,z)$ ， [37]

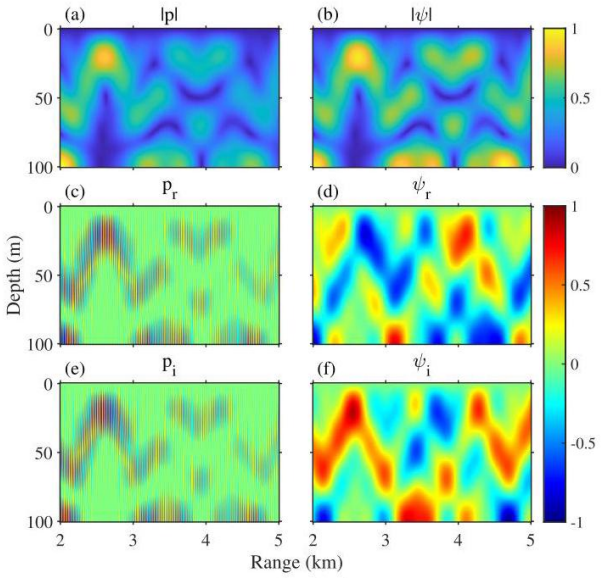

FIG. 1. (Color online) Normalized (a) and (b) magnitude, (c) and (d) real, and (e) and (f) imaginary of pressure field (left) and envelope field (right). The data are simulated in an isovelocity environment with a 100 Hz source at 25 m depth.

图 1.(彩色在线) 压力场 (左) 和包络场 (右) 的归一化 (a) 和 (b) 幅度、(c) 和 (d) 实部以及 (e) 和 (f) 虚部。数据是在等速环境中，在 25 m 深度处有一个 100 Hz 源的情况下模拟得到的。

J. Acoust. Soc. Am. 155 (3), March 2024 and smooth the pressure field. The envelope $\psi(r,z)$ is defined by Eq. (6.3) of Ref. 37,

《美国声学学会杂志》155(3)，2024 年 3 月并平滑压力场。包络 $\psi(r,z)$ 由参考文献 37 中的式 (6.3) 定义，

$$\psi(r,z) = p(r,z)/H_0^{(2)}(k_0 r), \tag{5}$$

where $k_0 = \omega/c_0$ is the reference wavenumber, c_0 is the reference sound speed, which is 1500 m/s . We name Eq. (5) as the envelope transform. In an ocean waveguide, the acoustic pressure field is dominated by modes with close mode wave-numbers. Mode wavenumber can be expressed as $k_m = \omega/c_m$, where c_m represents the phase velocity of m th mode. Since c_0 is close to c_m, k_0 is close to k_m , and an envelope transform can smooth the acoustic pressure field by decreasing a wavenumber to $k_m - k_0$. Figures 1(d) and 1(f) show a real and imaginary component of envelope ψ , exhibiting much smoother variation compared to the pressure field in Figs. 1(c) and 1(e). If c_0 is adjusted to reduce further $|k_m - k_0|$, a smoother envelope field is achieved. However, since $c_0 = 1500$ m/s significantly reduces the wavenumber, further adjustment yields marginal effects. Since the range of c_m is unknown, we set c_0 as 1500 m/s .

其中 $k_0 = \omega/c_0$ 是参考波数，c_0 是参考声速，其值为 1500 m/s 。我们将式 (5) 称为包络变换。在海洋波导中，声压场由波数相近的模式主导。模式波数可表示为 $k_m = \omega/c_m$ ，其中 c_m 表示第 m 模式的相速度。由于 c_0 接近 c_m, k_0 接近 k_m ，并且包络变换可以通过将波数降低到 $k_m - k_0$ 来平滑声压场。图 1(d) 和 1(f) 显示了包络 ψ 的实部和虚部，与图 1(c) 和 1(e) 中的压力场相比，其变化更加平滑。如果调整 c_0 以进一步降低 $|k_m - k_0|$ ，则可获得更平滑的包络场。然而，由于 $c_0 = 1500$ m/s 显著降低了波数，进一步调整产生的效果甚微。由于 c_m 的范围未知，我们将 c_0 设置为 1500 m/s 。

To overcome the second challenge, we use the magnitude of the envelope, which is easily converted from the magnitude of the pressure field. In far-field condition ($kr \gg 1$) , the magnitude of the envelope is expressed as

为了克服第二个挑战，我们使用包络的幅度，它很容易从压力场的幅度转换而来。在远场条件 ($kr \gg 1$) 下，包络的幅度表示为

$$|\psi(r,z)| = \sqrt{\frac{\pi k_0 r}{2}}\,|p(r,z)|\,. \tag{6}$$

Figure 1(b) shows the envelope magnitude. Unlike the pressure magnitude in Fig. 1(a), the envelope magnitude does not decrease with range, as it is compensated by a factor of $\sqrt{r}$.

图 1(b) 显示了包络幅度。与图 1(a) 中的压力幅度不同，包络幅度不会随距离减小，因为它由一个 $\sqrt{r}$ 因子进行了补偿。

The governing equation for envelope ψ is derived:

推导了包络 ψ 的控制方程:

Rewriting the Helmholtz equation in Eq. (1) as

将式 (1) 中的亥姆霍兹方程改写为

$$\frac{\partial^2 p}{\partial r^2} + \frac{1}{r}\frac{\partial p}{\partial r} + \frac{\partial^2 p}{\partial z^2} + k_0^2 n^2 p = 0, \tag{7}$$

where $n(r,z) = c_0/c(r,z)$ is the index of refraction. Substituting the pressure p into Eq. (7) by envelope ψ , and using that the Hankel function, satisfies the Bessel differential equation, [37]

其中 $n(r,z) = c_0/c(r,z)$ 是折射率。通过包络 ψ 将压力 p 代入式 (7)，并利用汉克尔函数满足贝塞尔微分方程 [37]

$$\frac{\partial^2 H_0^{(2)}(k_0 r)}{\partial r^2} + \frac{1}{r}\frac{\partial H_0^{(2)}(k_0 r)}{\partial r} + k_0^2 H_0^{(2)}(k_0 r) = 0, \tag{8}$$

gives

得到

$$\frac{\partial^2\psi}{\partial r^2}+\left(\frac{2}{H_0^{(2)}(k_0r)}\frac{\partial H_0^{(2)}(k_0r)}{\partial r}+\frac{1}{r}\right)\frac{\partial\psi}{\partial r}+\frac{\partial^2\psi}{\partial z^2}$$

$$+k_0^2\left(n^2-1\right)\psi=0. \tag{9}$$

Using Eq. (4), the governing equation for envelope function ψ is derived as [37]

利用式 (4)，推导出包络函数 ψ 的控制方程为 [37]

$$\mathcal{N}_\psi[\psi]\overset{\text{def}}{=}\frac{\partial^2\psi}{\partial r^2}-2ik_0\frac{\partial\psi}{\partial r}+\frac{\partial^2\psi}{\partial z^2}+k_0^2\left(n^2-1\right)\psi=0, \tag{10}$$

where $\mathcal{N}_\psi$ represents differential operator.

其中 $\mathcal{N}_\psi$ 表示微分算子。

C. Physics-informed neural networks

C. 基于物理信息的神经网络

PINN is a deep-learning framework for solving forward and inverse problems involving nonlinear PDEs. [1] PINN deals with general physics systems, characterized by a governing equation, Eq. (11), and a boundary condition, Eq. (12), that are satisfied within a domain Ω along its boundary $\partial\Omega$,

PINN 是一种深度学习框架，用于解决涉及非线性偏微分方程的正向和反向问题。[1] PINN 处理一般物理系统，其特征在于一个控制方程 (式 (11)) 和一个边界条件 (式 (12))，它们在一个域 Ω 内及其边界 $\partial\Omega$ 上满足，

$$\mathcal{N}[u(x)]=f(x)\ \ x\in\Omega, \tag{11}$$

$$\mathcal{B}[u(x)]=g(x)\ \ x\in\partial\Omega, \tag{12}$$

where x represents input coordinates, such as spatial and temporal dimensions, while u represents physical quantities, as pressure or velocity. $\mathcal{N}[\cdot]$ and $\mathcal{B}[\cdot]$ denote differential operator. Neural networks are universal function approxima-tors, [48] capable of representing any continuous function with the proper configuration and a sufficient number of neurons. For PINN, neural networks are used to approximate the solutions of PDEs, $u(x)$ (see Fig. 2).

其中 x 表示输入坐标，如空间和时间维度，而 u 表示物理量，如压力或速度。$\mathcal{N}[\cdot]$ 和 $\mathcal{B}[\cdot]$ 表示微分算子。神经网络是通用函数逼近器，[48] 能够通过适当的配置和足够数量的神经元来表示任何连续函数。对于 PINN，神经网络用于逼近偏微分方程的解，$u(x)$ (见图 2)。

A limited set of input-output pairs $\left\{x_m^i, u\left(x_m^i\right)\right\}_{i=1}^{N_m}$ is known, obtained from initial conditions or measurements. There are three sources of information to solve the problem: (1) a limited number of known input-output pairs, (2) the governing equation, and (3) the boundary condition. It is important to note that even with limited data, leveraging the system's underlying physics allows us to compensate for sparse datasets. Contrasting with purely data-driven machine learning methods that depend solely on a limited dataset of input-output pairs, PINNs integrate physical principles into their loss function. This integration enables the PINN to effectively solve problems, even with a small amount of dataset.

已知从初始条件或测量中获得了一组有限的输入 - 输出对 $\left\{x_m^i, u\left(x_m^i\right)\right\}_{i=1}^{N_m}$。有三种信息来源可用于解决该问题:(1) 有限数量的已知输入 - 输出对，(2) 控制方程，以及 (3) 边界条件。需要注意的是，即使数据有限，利用系统的基础物理知识也能让我们弥补稀疏数据集的不足。与仅依赖有限输入 - 输出对数据集的纯数据驱动机器学习方法不同，PINN 将物理原理集成到其损失函数中。这种集成使 PINN 即使在数据集较少的情况下也能有效解决问题。

PINNs are trained with a composite loss function,

PINN 使用复合损失函数进行训练,

$$\mathcal{L}(\theta) = \lambda_M \mathcal{L}_{\mathcal{M}}(\theta) + \lambda_B \mathcal{L}_{\mathcal{B}}(\theta) + \lambda_N \mathcal{L}_{\mathcal{N}}(\theta), \tag{13}$$

where λ_M, λ_B , and λ_N are weighting coefficients and θ is trainable parameters of neural network. Neural network parameters are updated using gradient-descent methods based on the backpropagation of the loss function. Each loss term is expressed as

其中 λ_M, λ_B 和 λ_N 是加权系数，θ 是神经网络的可训练参数。神经网络参数使用基于损失函数反向传播的梯度下降方法进行更新。每个损失项表示为

$$\mathcal{L}_{\mathcal{M}}(\theta) = \frac{1}{N_m} \sum_{i=1}^{N_m} \left|\hat{u}\left(x_m^i; \theta\right) - u\left(x_m^i\right)\right|^2, \tag{14}$$

$$\mathcal{L}_{\mathcal{B}}(\theta) = \frac{1}{N_b} \sum_{i=1}^{N_b} \left|\mathcal{B}\left[\hat{u}\left(x_b^i; \theta\right)\right] - g\left(x_b^i\right)\right|^2, \tag{15}$$

$$\mathcal{L}_{\mathcal{N}}(\theta) = \frac{1}{N_n} \sum_{i=1}^{N_n} \left|\mathcal{N}\left[\hat{u}\left(x_n^i; \theta\right)\right] - f\left(x_n^i\right)\right|^2. \tag{16}$$

$\mathcal{L}_{\mathcal{M}}, \mathcal{L}_{\mathcal{B}}$, and $\mathcal{L}_{\mathcal{N}}$ have a distinct role: fitting the neural network to the known data, enforcing the boundary condition, and the governing equation. Traditional neural networks rely solely on a data-based loss function, $\mathcal{L}_{\mathcal{M}}$. In contrast, PINNs incorporate physics-based losses, $\mathcal{L}_{\mathcal{B}}$ and $\mathcal{L}_{\mathcal{N}}$. These losses are evaluated at different sets of data points, including known points $\left\{x_m^i\right\}_{i=1}^{N_m}$, boundary points $\left\{x_b^i\right\}_{i=1}^{N_b}$, and collocation points $\left\{x_n^i\right\}_{i=1}^{N_n}$. Boundary and collocation points are specific sampling locations to enforce the boundary condition and the governing PDE. These points are strategically sampled from the boundary $\partial\Omega$ and the domain Ω of the physics problem, respectively. The number of these sampling points, N_n for collocation and N_b for boundary points, can be freely selected. The differential operator $\mathcal{B}[\cdot]$ and $\mathcal{N}[\cdot]$ can be easily calculated since neural networks can efficiently compute gradients of the outputs with respect to the inputs, $\partial\hat{u}/\partial x$, via automatic differentiation. [49] This enables computing loss terms $\mathcal{L}_{\mathcal{B}}$ and $\mathcal{L}_{\mathcal{N}}$.

$\mathcal{L}_{\mathcal{M}}, \mathcal{L}_{\mathcal{B}}$ 和 $\mathcal{L}_{\mathcal{N}}$ 具有不同的作用: 使神经网络拟合已知数据、施加边界条件以及控制方程。传统神经网络仅依赖基于数据的损失函数 $\mathcal{L}_{\mathcal{M}}$。相比之下，PINN 纳入了基于物理的损失 $\mathcal{L}_{\mathcal{B}}$ 和 $\mathcal{L}_{\mathcal{N}}$。这些损失在不同的数据点集上进行评估，包括已知点 $\{x_m^i\}_{i=1}^{N_m}$、边界点 $\{x_b^i\}_{i=1}^{N_b}$ 和配置点 $\{x_n^i\}_{i=1}^{N_n}$。边界点和配置点是用于施加边界条件和控制偏微分方程的特定采样位置。这些点分别从物理问题的边界 $\partial\Omega$ 和域 Ω 中进行策略性采样。这些采样点的数量，配置点为 N_n，边界点为 N_b，可以自由选择。由于神经网络可以通过自动微分有效地计算输出相对于输入 $\partial\hat{u}/\partial x$ 的梯度，因此微分算子 $\mathcal{B}[\cdot]$ 和 $\mathcal{N}[\cdot]$ 可以轻松计算。[49] 这使得能够计算损失项 $\mathcal{L}_{\mathcal{B}}$ 和 $\mathcal{L}_{\mathcal{N}}$。

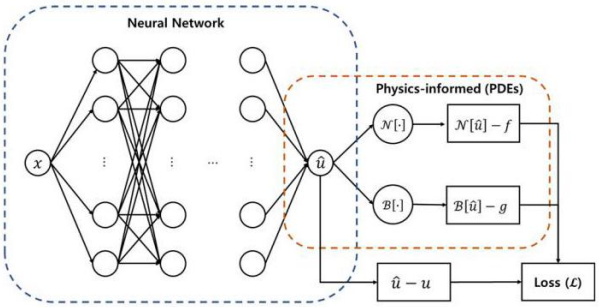

FIG. 2. (Color online) The general PINN framework.

图 2.(在线彩色) 通用的 PINN 框架。

D. OceanPINN

D. OceanPINN

We propose OceanPINN, an approach that harnesses PINN[1] to reconstruct the unmeasured acoustic field in ocean waveguides, using partially measured data. Due to the sensitivity of the phase, we exclusively use the magnitude from the measured data. As depicted in Fig. 3(a), acoustic magnitudes are transformed into envelope magnitudes using Eq. (6) before training.

我们提出了 OceanPINN，一种利用 PINN[1] 使用部分测量数据重建海洋波导中未测量声场的方法。由于相位的敏感性，我们仅使用测量数据的幅度。如图 3(a) 所示，在训练之前，使用式 (6) 将声学幅度转换为包络幅度。

In the OceanPINN, the fully connected neural network receives a range-depth (r, z) as input and outputs the real and imaginary envelope $\widehat{\psi}_{\mathrm{r}}(r, z)$ and $\widehat{\psi}_{\mathrm{i}}(r, z)$ at the input location (r, z) , as Fig. 3(c). The complex envelope is formed from these outputs as $\widehat{\psi} = \widehat{\psi}_{\mathrm{r}} + i\widehat{\psi}_{\mathrm{i}}$. After training, the neural network generates the envelope $\widehat{\psi}(r, z)$ for specific points (r, z) . The pressure field $\hat{p}(r, z)$ is then estimated by multiplying the estimated envelope $\widehat{\psi}(r, z)$ with the Hankel function $H_0^{(2)}(k_0 r)$.

在海洋 PINN 中，全连接神经网络接收距离-深度 (r, z) 作为输入，并在输入位置 (r, z) 输出实部和虚部包络 $\widehat{\psi}_{\mathrm{r}}(r, z)$ 和 $\widehat{\psi}_{\mathrm{i}}(r, z)$，如图 3(c) 所示。复包络由这些输出按 $\widehat{\psi} = \widehat{\psi}_{\mathrm{r}} + i\widehat{\psi}_{\mathrm{i}}$ 形成。训练后，神经网络为特定点 (r, z) 生成包络 $\widehat{\psi}(r, z)$。然后通过将估计的包络 $\widehat{\psi}(r, z)$ 与汉克尔函数 $H_0^{(2)}(k_0 r)$ 相乘来估计压力场 $\hat{p}(r, z)$。

A fully connected neural network with L hidden layers, an input layer (layer 0), and an output layer (layer $L+1$) is used for the OceanPINN [see Fig. 3(c)]. We apply the sine activation functions because it is effective in representing the complex signals and their derivative. [50] In addition, adopting sine activation is effective for solving the Helmholtz Equation. [27,50] The network can be expressed as

具有 L 个隐藏层、一个输入层 (第 0 层) 和一个输出层 (第 $L+1$ 层) 的全连接神经网络用于海洋 PINN[见图 3(c)]。我们应用正弦激活函数，因为它在表示复信号及其导数方面很有效。[50] 此外，采用正弦激活对于求解亥姆霍兹方程是有效的。[27,50] 该网络可以表示为

$$x_{l+1} = \begin{cases} \sin\left(W_l x_l + b_l\right), & l = 0, \ldots, L-1, \\ W_l x_l, & l = L, \end{cases} \tag{17}$$

where x_l denotes the l th layer and W_l and b_l denote the weight and bias connecting the layer l and $l+1$.

其中 x_l 表示第 l 层，W_l 和 b_l 表示连接第 l 层和 $l+1$ 层的权重和偏差。

We use three sources of information: (1) measured data, (2) the governing equation [Eq. (10)], and (3) the pressure release surface boundary condition with $\psi(r,0)=0$. Each information is incorporated into the loss function as

我们使用三种信息来源:(1) 测量数据，(2) 控制方程 [式 (10)]，以及 (3) 具有 $\psi(r,0)=0$ 的压力释放表面边界条件。每种信息都被纳入损失函数，如下所示

$$\mathcal{L}_{\mathcal{M}} = \frac{1}{N_m}\sum_{i=1}^{N_m}\left|\widehat{\psi}_{\mathrm{r}}^2\left(r_m^i, z_m^i\right) + \widehat{\psi}_{\mathrm{i}}^2\left(r_m^i, z_m^i\right) - \left|\psi\left(r_m^i, z_m^i\right)\right|^2\right|, \tag{18}$$

$$\mathcal{L}_{\mathcal{B}} = \frac{1}{N_b}\sum_{i=1}^{N_b}\left|\widehat{\psi}\left(r_b^i, 0\right)\right|^2, \tag{19}$$

$$\mathcal{L}_{\mathcal{N}} = \frac{1}{N_n}\sum_{i=1}^{N_n}\left|\mathcal{N}_\psi\left[\widehat{\psi}\left(r_n^i, z_n^i\right)\right]\right|^2. \tag{20}$$

Here, neural network parameters θ are omitted for simplicity. Note that in Eq. (18), since only the magnitude of the measured data is available, the neural network outputs are compared with the magnitude square. Losses are combined as in Eq. (13) and used to train OceanPINN.

这里，为了简单起见，省略了神经网络参数 θ。请注意，在式 (18) 中，由于只有测量数据的幅度可用，因此将神经网络输出与幅度平方进行比较。损失按照式 (13) 进行组合，并用于训练海洋 PINN。

Training points are depicted in Fig. 3(c). Boundary points are evenly sampled from the water surface, and collocation points are sampled from the water medium differently in each iteration to prevent the PINN from being trapped in local minima. [51] Further details on the sampling method for collocation points are shown in Appendix A.

训练点如图 3(c) 所示。边界点从水面均匀采样，配置点在每次迭代中从水介质中不同地采样，以防止 PINN 陷入局部最小值。[51] 配置点采样方法的更多细节见附录 A。

We utilize the following hyperparameters: loss weight coefficients are set as $\lambda_M = 1, \lambda_N = 10^5, \lambda_B = 1$. Further details for loss weight coefficients are provided in Appendix B. The number of training points, N_n and N_b , are set to 3000 and 100, respectively. The network architecture comprises $L = 5$ hidden layers, each with 160 neurons. The loss function is optimized using the Adam optimizer with a learning rate of 10^{-4} . We multiplied the loss function by 10^4 arbitrarily, which improved the convergence speed and model performance of analyzed cases. This adjustment aims to prevent overly small gradients, reducing the likelihood of the model falling into local minima.

我们使用以下超参数: 损失权重系数设置为 $\lambda_M = 1, \lambda_N = 10^5, \lambda_B = 1$ 。损失权重系数的更多细节见附录 B。训练点的数量 N_n 和 N_b 分别设置为 3000 和 100。网络架构包括 $L = 5$ 个隐藏层，每层有 160 个神经元。使用学习率为 10^{-4} 的 Adam 优化器对损失函数进行优化。我们任意地将损失函数乘以 10^4 ，这提高了分析案例的收敛速度和模型性能。这种调整旨在防止梯度过小，降低模型陷入局部最小值的可能性。

III. ISOVELOCITY PROBLEM

III. 等声速问题

This section evaluates and compares the performance of OceanPINN with other representative machine-learning frameworks. We consider a simple problem characterized by an isovelocity profile, constant density, and boundary conditions including a pressure-release surface and a rigid bottom, as outlined in Chapter 5.4 of Ref. 37 (see Fig. 4). The acoustic pressure field is generated using Eq. (5.49) from Ref. 37. The first four of the 13 propagating modes are considered for simulation following the example presented in Refs. 37 and 52. The pressure field is generated across a range of $2 - 5$ km . The sound pressure level (SPL) of the simulated pressure field is presented in Fig. 5(a), which is normalized by its maximum value.

本节评估并比较海洋 PINN 与其他代表性机器学习框架的性能。我们考虑一个简单的问题，其特征是等声速剖面、恒定密度以及包括压力释放表面和刚性底部的边界条件，如参考文献 37 的第 5.4 章所述 (见图 4)。声压场使用参考文献 37 中的式 (5.49) 生成。按照参考文献 37 和 52 中的示例，在模拟中考虑了 13 个传播模式中的前四个。在 $2 - 5$ km 的范围内生成压力场。模拟压力场的声压级 (SPL) 如图 5(a) 所示，其通过最大值进行归一化。

To assess the predictive performance in unsampled range-depths, we sample pressure magnitudes while excluding certain depths and ranges. For depth, pressure magnitudes are sampled at 5 m intervals, specifically between 5 and 30 m and $80-95$ m . For ranges, pressure magnitudes are sampled at 25 m intervals over 600 m , and the next 400 m is unsampled. This pattern is repeated. Dashed boxes in Figs. 5(b)-5(d) illustrate the sampled regions.

为了评估未采样距离深度下的预测性能，我们在排除某些深度和范围的同时对压力幅值进行采样。对于深度，压力幅值以 5 m 间隔进行采样，具体为 5 到 30 m 以及 80 – 95 m 之间。对于范围，压力幅值在 600 m 上以 25 m 间隔进行采样，接下来的 400 m 未被采样。此模式重复进行。图 5(b) - 5(d) 中的虚线框展示了采样区域。

The predictive performance is quantitatively assessed by the mean absolute error (MAE) of SPL, defined as

预测性能通过声压级的平均绝对误差 (MAE) 进行定量评估，定义为

$$\mathrm{MAE} = \frac{1}{n}\sum_{i=1}^{n}\left|L_p^i - \hat{L}_p^i\right|, \tag{21}$$

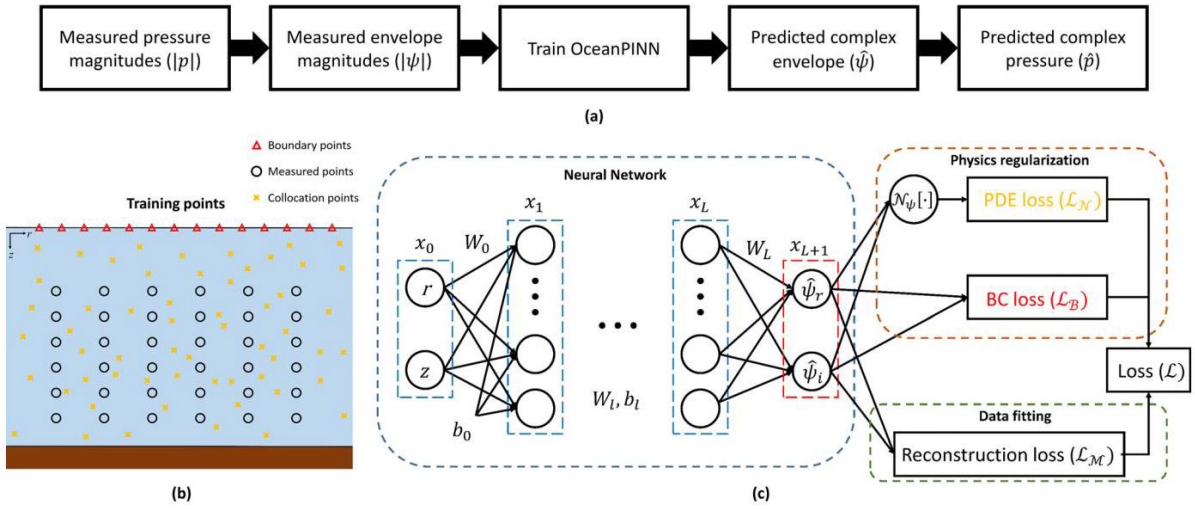

FIG. 3. (Color online) (a) Flowchart, (b) training points, (c) schematic of the OceanPINN.

图 3.(彩色在线)(a) 流程图，(b) 训练点，(c) 海洋 PINN 示意图。

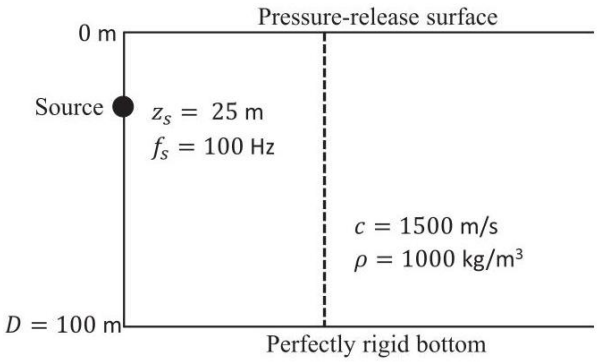

FIG. 4. Schematic of the isovelocity problem.

图 4. 等速问题示意图。

where $\hat{L}_p$ and L_p are the predicted and true SPL, n is the total number of evaluated points, and i indexes the individual points. For the isovleocity problem, evaluation points are uniformly distributed on the (r, z) grid at 10 m and 1 m intervals, respectively. Surface points are excluded due to the SPL being negative infinity, i.e., $p(r, 0) = 0$.

其中 $\hat{L}_p$ 和 L_p 分别为预测声压级和真实声压级，n 为评估点总数，i 为各个点的索引。对于等速问题，评估点分别以 10 m 和 1 m 间隔均匀分布在 (r, z) 网格上。由于声压级为负无穷大，即 $p(r, 0) = 0$ ，所以表面点被排除。

A. Results

A. 结果

Three machine learning methods are evaluated, including the proposed OceanPINN. Two methods are compared with OceanPINN, all employing the same neural network architecture but differing in their outputs and loss functions. Specifically, whereas OceanPINN outputs the envelope $\widehat{\psi}$, two other methods output the pressure $\widehat{p}$. The first method for comparison is a purely data-driven approach, trained solely using reconstruction loss where ψ of Eq. (18) is replaced by p . The second method for comparison is a PINN that outputs the pressure. This method is trained with composite loss similar to OceanPINN, which replaces the ψ to p in Eq. (18) and Eq. (19), and Eq. (20) is revised to enforce the original Helmholtz equation in Eq. (7). To keep the loss functions on equal footing, we empirically choose $\lambda_M = \lambda_N = \lambda_B = 1$, in agreement with Ref. 23.

评估了三种机器学习方法，包括所提出的海洋 PINN。将两种方法与海洋 PINN 进行比较，它们都采用相同的神经网络架构，但输出和损失函数不同。具体而言，海洋 PINN 输出包络 $\widehat{\psi}$，而另外两种方法输出压力 $\widehat{p}$。第一种比较方法是纯数据驱动方法，仅使用重建损失进行训练，其中式 (18) 中的 ψ 被 p 取代。第二种比较方法是输出压力的 PINN。该方法使用与海洋 PINN 类似的复合损失进行训练，它取代了式 (18)、式 (19) 中的 ψ 至 p ，并且式 (20) 被修订以强制执行式 (7) 中的原始亥姆霍兹方程。为使损失函数处于同等基础，我们根据参考文献 23 经验性地选择 $\lambda_M = \lambda_N = \lambda_B = 1$ 。

These methods are trained over 500000 epochs using pressure magnitude samples, and after training, they predict the complex pressure field in the entire domain. The magnitude of the predicted pressure field and the phase difference from the true field are presented in Figs. 5(b)-5(d). The SPL figures are normalized to the maximum value of the true pressure field. The homogeneous Helmholtz equation allows multiple solutions with constant phase shifts θ . For instance, if $p(r, z)$ is a solution, then $p(r, z)\, e^{i\theta}$ is a valid solution. Since phase information is not provided, the predicted field can exhibit a constant phase difference from the true field. Note that these predictions with a constant phase difference, still qualify as PDE solutions and are spatially coherent.

这些方法使用压力幅值样本在 500000 个轮次上进行训练，训练后，它们预测整个域中的复压力场。预测压力场的幅值以及与真实场的相位差在图 5(b) - 5(d) 中呈现。声压级图已归一化为真实压力场的最大值。齐次亥姆霍兹方程允许具有恒定相移 θ 的多个解。例如，如果 $p(r, z)$ 是一个解，那么 $p(r, z)\, e^{i\theta}$ 是一个有效解。由于未提供相位信息，预测场可能与真实场呈现恒定的相位差。请注意，这些具有恒定相位差的预测仍然符合偏微分方程解的条件并且在空间上是相干的。

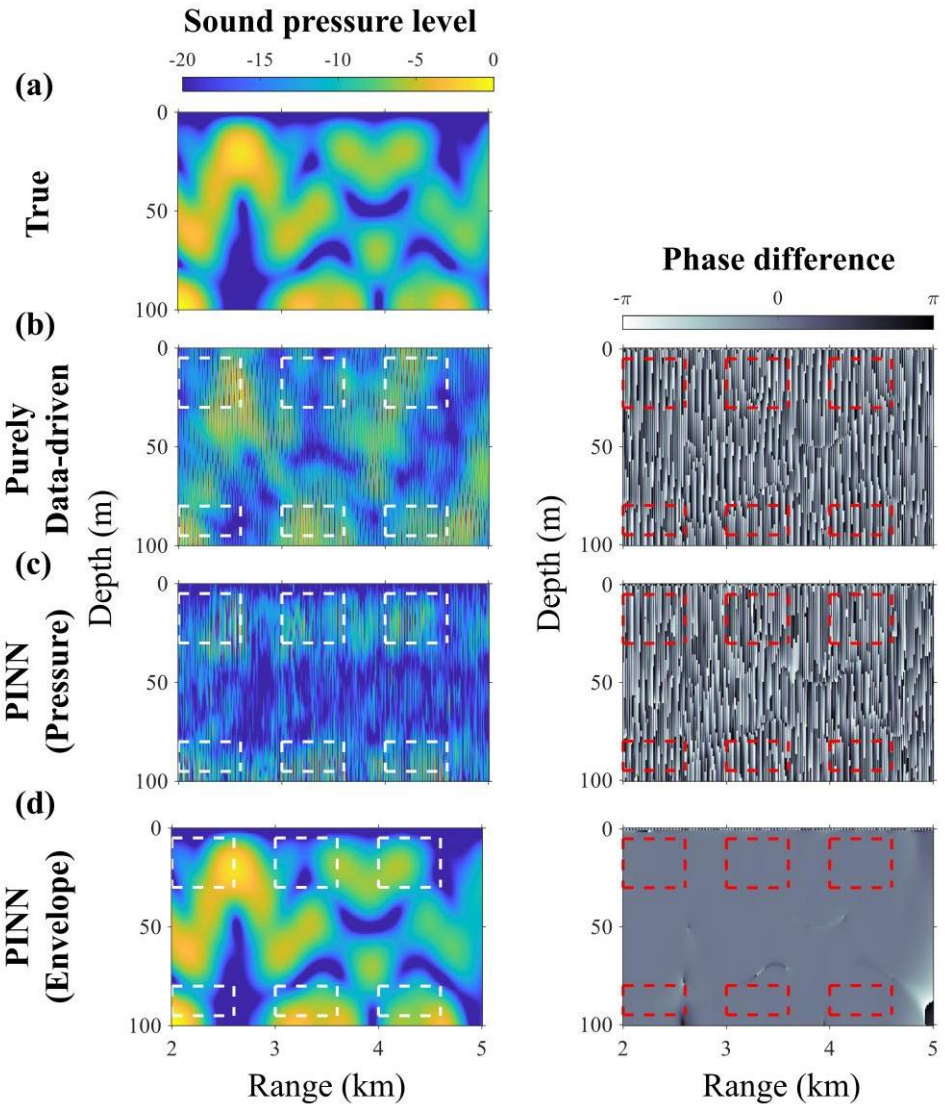

FIG. 5. (Color online) (Left) The normalized sound pressure level (dB), (Right) phase difference between true and predicted pressure field. Each row illustrates (a) true, (b) purely data-driven method, (c) PINN with pressure output, (d) PINN with envelope output (OceanPINN). Dashed boxes represent the sampled region.

图 5.(彩色在线)(左) 归一化声压级 (dB)，(右) 真实压力场与预测压力场之间的相位差。每行展示 (a) 真实情况, (b) 纯数据驱动方法, (c) 输出压力的 PINN, (d) 输出包络的 PINN(海洋 PINN)。虚线框表示采样区域。

Figures 5(b) and 5(c) present the prediction results of the compared methods, showing significant discrepancies from the true values in both magnitude and phase. The predicted SPLs in Figs. 5(b) and 5(c) are inaccurate even in the sampled region. This inaccuracy is attributed to the relatively sparse sampling intervals, which are insufficient for neural networks to capture the highly fluctuating nature of complex ocean acoustic pressure fields. In contrast, OceanPINN predictions in Fig. 5(d) are accurate in both magnitude and

phase. The proposed method achieves significantly lower MAE than other methods, as shown in Table I. The phase differences are consistent across the entire region, except in the small areas where the magnitude is close to zero, where we can neglect the phase. These results demonstrate the effectiveness of the proposed PINN framework using the envelope field. However, OceanPINN also exhibits inaccuracies around 5 km , near the bottom, highlighting the inherent challenges PINNs face with extrapolation. [53]

图 5(b) 和 5(c) 展示了对比方法的预测结果，在幅值和相位上均与真实值存在显著差异。即使在采样区域，图 5(b) 和 5(c) 中预测的声压级也不准确。这种不准确性归因于相对稀疏的采样间隔，这对于神经网络捕捉复杂海洋声压场的高度波动特性来说是不够的。相比之下，图 5(d) 中的 OceanPINN 预测在幅值和相位上都是准确的。如表 I 所示，所提出的方法实现了比其他方法显著更低的平均绝对误差 (MAE)。除了幅值接近零的小区域 (在这些区域我们可以忽略相位) 外，整个区域的相位差是一致的。这些结果证明了所提出的使用包络场的 PINN 框架的有效性。然而，OceanPINN 在 5 km 附近、靠近海底的区域也表现出不准确，突出了 PINN 在进行外推时面临的固有挑战。[53]

IV. SWELLEX-96

四、SWELLEX - 96

We evaluate the OceanPINN in a more realistic environment. The analysis utilizes both simulation and experimental data from the SWellEx-96 Event S5[54–57] environment, which was conducted at 23:15-00:30 UTC from May 10-11, 1996. A brief overview of the SWellEx- 96 experiment and the specific source-receiver configuration used for the training data is provided.

我们在更现实的环境中评估 OceanPINN。该分析利用了 1996 年 5 月 10 日至 11 日协调世界时 23:15 - 00:30 进行的 SWellEx - 96 事件 S5[54–57] 环境的模拟和实验数据。提供了 SWellEx - 96 实验的简要概述以及用于训练数据的特定源 - 接收器配置。

During the experiment, the source ship simultaneously towed two sources: the shallow source and the deep source, each transmitting different multi-tonal sets. Here, we focus on the 109 Hz shallow source towed at a 9 m depth. The data were recorded by a 64-element VLA spanning depths of 94.125-212.25 m. A subset of the VLA comprising 13 evenly spaced elements (from elements 1-61) was selected for constructing the training dataset. The dataset incorporates data from transmissions originating between 1.5 and 3.5 km from the VLA, excluding ranges of $2.1-2.3$ km and 2.7-2.9 km. Source-receiver configuration for training data is illustrated in Fig. 6(a).

在实验期间，源船同时拖曳两个声源: 浅声源和深深源，每个声源发射不同的多音调集。在这里，我们关注在 9 m 深度拖曳的 109 Hz 浅声源。数据由一个跨越深度为 94.125 至 212.25 米的 64 元垂直线列阵 (VLA) 记录。选择 VLA 中包含 13 个均匀间隔元素 (从元素 1 - 61) 的子集来构建训练数据集。该数据集纳入了来自 VLA 在 1.5 至 3.5 km 之间发射的数据，不包括 $2.1-2.3$ km 和 2.7 - 2.9 千米的范围。训练数据的源 - 接收器配置如图 6(a) 所示。

We assumed a range-independent environment, consistent with previous studies. [43,44,52,58] With N_r range samples and 13 hydrophones, we can obtain $N_r \times 13$ different magnitude pressure field measurements, denoted as $\left|p\left(r_i, z_j\right)\right|$ for $1 \leq i \leq N_r, 1 \leq j \leq 13$, where r_i represents the distance

我们假设了一个与距离无关的环境，这与之前的研究一致。[43,44,52,58] 使用 N_r 距离样本和 13 个水听器，我们可以获得 $N_r \times 13$ 不同幅度的压力场测量值，对于 $1 \le i \le N_r, 1 \le j \le 13$ 表示为 $|p(r_i, z_j)|$，其中 r_i 代表距离

TABLE I. MAE of the predicted pressure field in Figs. 5(b)-5(d).

表 I. 图 5(b) - 5(d) 中预测压力场的平均绝对误差 (MAE)。

Method	MAE (dB)
Purely data-driven	5.65
PINN (Pressure)	7.58
OceanPINN	0.50

方法	平均绝对误差 (dB)
纯数据驱动	5.65
物理信息神经网络 (压力)	7.58
海洋物理信息神经网络	0.50

J. Acoust. Soc. Am. 155 (3), March 2024 between the i th transmission source and j th hydrophone at depth z_j . These measurement points are illustrated as white points in Fig. 6(a). The number of range samples, N_r differs between simulation and experiment. The measured pressure magnitude $|p|$ is converted to the envelope magnitude $|\psi|$ according to Eq. (6) and used to train OceanPINN.

《美国声学学会杂志》155(3)，2024 年 3 月，在深度为 z_j 处，i 号发射源与 j 号水听器之间。这些测量点在图 6(a) 中以白点表示。距离样本数量 N_r 在模拟和实验中有所不同。根据式 (6) 将测量的压力幅值 $|p|$ 转换为包络幅值 $|\psi|$，并用于训练 OceanPINN。

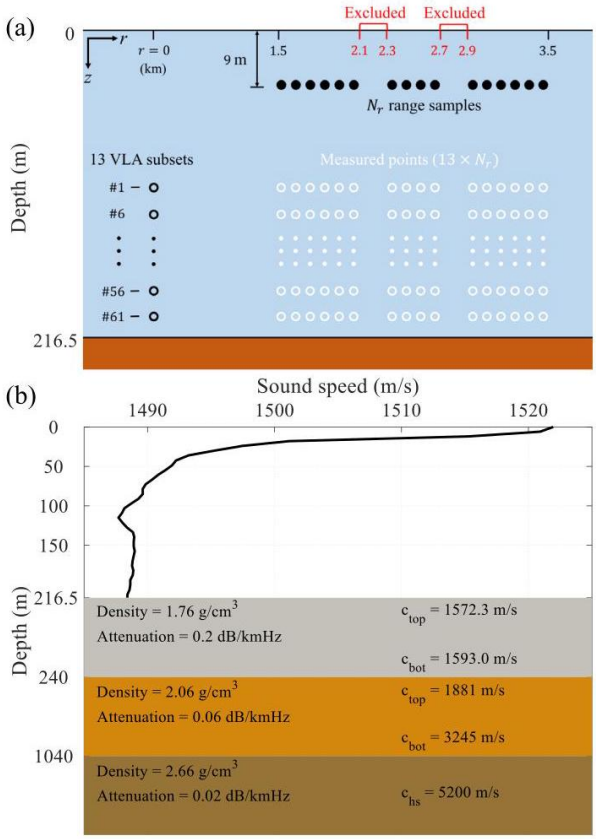

FIG. 6. (Color online) (a) Source-receiver configuration for the training dataset, (b) environmental parameters of the SWellEx-96 experiment.

图 6。(彩色在线)(a) 训练数据集的源 - 接收器配置，(b)SWellEx - 96 实验的环境参数。

A. SWellEx-96 simulation data generation

A. SWellEx - 96 模拟数据生成

In the simulation, the data are sampled in 20 m range intervals and yields a total of $N_r \times N_z = 83 \times 13$ samples for training. We used the Kraken normal mode model [47] to simulate the acoustic pressure field. Bottom attenuation influences the effective mode cutoff, and using an incorrect number of propagating modes can lead to mismatches between replicas and experimental data. [55,59] Accordingly, we conducted SWellEx-96 109 Hz simulations using 14 modes, as in the experimental data. The environmental parameters used for simulation are illustrated in Fig. 6(b).

在模拟中，数据在 20 m 个距离区间内采样，总共产生 $N_r \times N_z = 83 \times 13$ 个用于训练的样本。我们使用 Kraken 简正波模型 [47] 来模拟声压场。海底衰减会影响有效模式截止，使用不正确的传播模式数量可能导致副本与实验数据之间的不匹配。[55,59] 因此，我们像实验数据一样，使用 14 个模式进行了 SWellEx - 96 109 Hz 的模拟。用于模拟的环境参数如图 6(b) 所示。

OceanPINN is assessed across various signal-to-noise ratios (SNRs) of 12 and 6 dB , including noiseless conditions. In noisy scenarios, Gaussian noise is added to the generated pressure data. SNR is defined as

OceanPINN 在 12 和 6 dB 的各种信噪比 (SNR) 下进行评估，包括无噪声条件。在有噪声的情况下，高斯噪声被添加到生成的压力数据中。SNR 定义为

$$SNR = 20\log_{10}\frac{\left\|P_s\right\|_F}{\left\|P_n\right\|_F}, \tag{22}$$

where $\|\cdot\|_F$ is Frobenius norm, and $P_s \in \mathbb{C}^{N_r \times N_z}$ and $P_n \in \mathbb{C}^{N_r \times N_z}$ represent the noiseless measurement and additive noise at N_r range samples and N_z depth samples.

其中 $\|\cdot\|_F$ 是弗罗贝尼乌斯范数，$P_s \in \mathbb{C}^{N_r \times N_z}$ 和 $P_n \in \mathbb{C}^{N_r \times N_z}$ 分别表示在 N_r 个距离样本和 N_z 个深度样本处的无噪声测量值和加性噪声。

B. SWellEx-96 simulation results

B. SWellEx - 96 模拟结果

OceanPINN is trained over 1200000 epochs. After training, the pressure field is generated on a uniform (r, z) grid. The grid spans from 1 to 4 km for r at 10 m intervals and from 0 to 216.5 m for z with 300 uniformly spaced points.

OceanPINN 在 1200000 个轮次上进行训练。训练后，在均匀的 (r, z) 网格上生成压力场。对于 r ，网格在 10 m 间隔下从 1 跨度到 4 km ，对于 z ，从 0 跨度到 216.5 m ，有 300 个均匀分布的点。

Figures 7(b)-7(d) present predicted pressure magnitude fields, beamformings, and phase differences by OceanPINN, trained with data from various SNRs. All pressure magnitude figures are normalized to the maximum value of the true pressure field, and the beamforming figures are scaled to their maximum values. For easier comparison, each phase difference figure has been shifted by a constant phase to make the average phase difference zero.

图 7(b) 至 7(d) 展示了 OceanPINN 使用来自各种 SNR 的数据训练后预测的压力幅值场、波束形成和相位差。所有压力幅值图都归一化为真实压力场的最大值，波束形成图按其最大值进行缩放。为了便于比较，每个相位差图都通过一个恒定相位进行了偏移，以使平均相位差为零。

The predicted SPLs from OceanPINN are consistent with the true field across all SNRs. However, as previously discussed in Sec. IV A, discrepancies are observed in the extrapolated range of $3.5 - 4$ km . Table II provides a detailed quantitative analysis. MAEs increase in every SNRs as the predicted range extends from 1.5-3.5 km to 1-4 km.

OceanPINN 预测的声压级在所有 SNR 下都与真实场一致。然而，如第四节 A 中先前讨论的，在 $3.5 - 4$ km 的外推范围内观察到差异。表二提供了详细定量分析。随着预测范围从 1.5 - 3.5 千米扩展到 1 - 4 千米在每个 SNR 下平均绝对误差 (MAE) 都增加。

We validated the physical consistency of the predicted pressure field by the direction of arrival (DOA) in the beamforming figures. [54,56] We applied conventional beamforming to the predicted pressure fields. OceanPINN accurately predicts DOA within the interpolated range of $1.5-3.5$ km , affirming the physical consistency of its pressure field predictions. However, beamforming results of OceanPINN show discrepancies at $3.5-4$ km , showing limitations in extrapolating over longer ranges.

我们通过波束形成图中的到达方向 (DOA) 验证预测压力场的物理一致性。[54,56] 我们将传统波束形成应用于预测压力场。OceanPINN 在 $1.5-3.5$ km 的插值范围内准确预测 DOA，证实了其压力场预测的物理一致性。然而，OceanPINN 的波束形成结果在 $3.5-4$ km 处显示出差异，表明在更长范围外推时存在局限性。

The phase differences depicted in Figs. 7(b) -7(d) are nearly zero across the entire region within the interpolated range of $1.5-3.5$ km , indicating precise phase estimation. Discontinuities in these figures correspond with regions where the pressure magnitude is negligible or zero, which leads to phase values becoming indeterminate. In noisy conditions, such discontinuities become more prominent, since noise can mask the low-magnitude areas. In the extended range, the phase error increases, also showing challenges in range extrapolation.

图 7(b)-7(d) 所示的相位差在 $1.5-3.5$ km 插值范围内的整个区域几乎为零，表明相位估计精确。这些图中的不连续点对应于压力幅值可忽略或为零的区域，这导致相位值变得不确定。在有噪声的情况下，这种不连续点变得更加明显，因为噪声会掩盖低幅值区域。在扩展范围内，相位误差增大，这也表明在范围外推方面存在挑战。

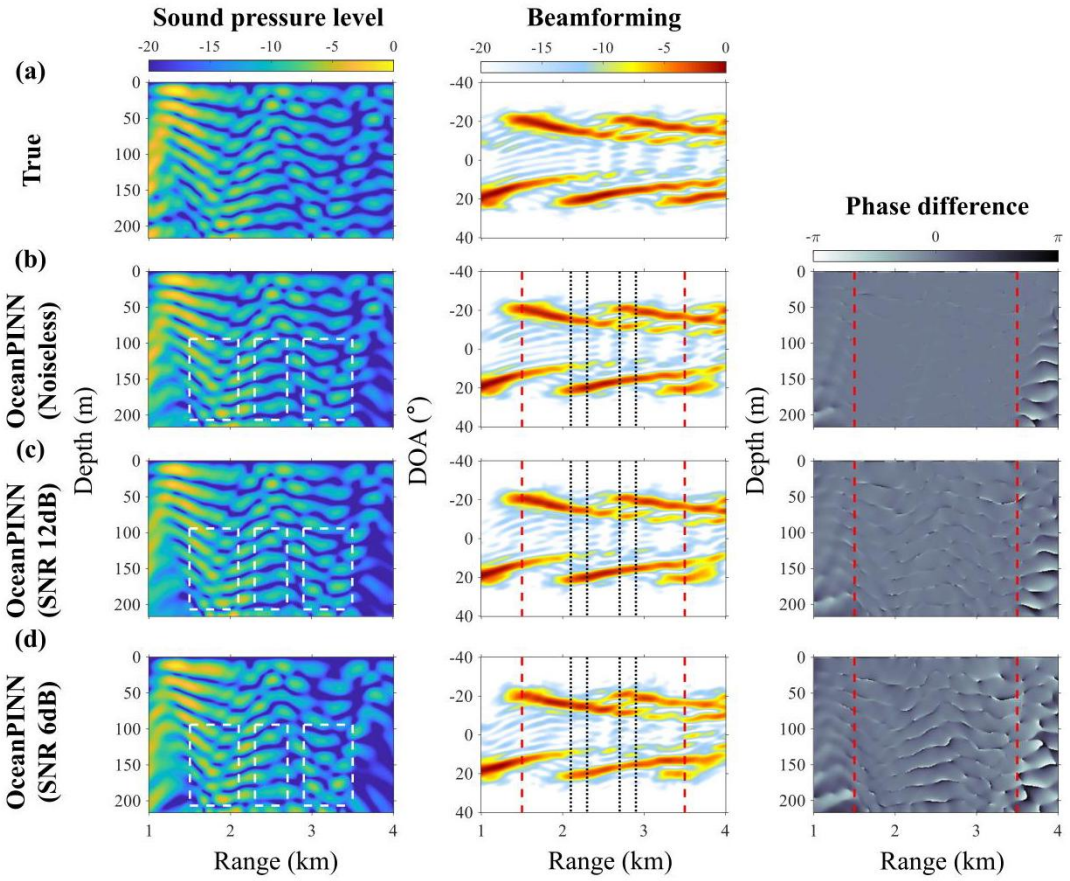

FIG. 7. (Color online) (Left) The normalized sound pressure level (dB), (Middle) beamforming (dB), and (Right) phase difference between true and predicted pressure field. Each row illustrates (a) true and OceanPINN prediction using (b) noiseless, (c) SNR 12 dB, (d) SNR 6 dB simulation data. Dashed and dotted lines represent the boundaries of sampled data.

图 7。(彩色在线)(左) 归一化声压级 (dB)，(中) 波束形成 (dB)，以及 (右) 真实压力场与预测压力场之间的相位差。每行展示了 (a) 真实情况和使用 (b) 无噪声、(c) 信噪比 12 dB、(d) 信噪比 6 dB 模拟数据的 OceanPINN 预测。虚线和点线表示采样数据的边界。

TABLE II. MAE of the predicted pressure field in Figs. 7(b)-7(d): Evaluated in the interpolated range of $1.5-3.5$ km and the extended range of $1-4$ km .

表 II。图 7(b)-7(d) 中预测压力场的平均绝对误差: 在 $1.5-3.5$ km 的插值范围和 $1-4$ km 的扩展范围内评估。

Meausurement SNR	MAE (dB)	
	1.5-3.5 km	1-4 km
Noiseless	0.18	0.68
12 dB	0.87	1.44
6 dB	1.83	2.38

测量信噪比	平均绝对误差 (dB)	
	1.5 - 3.5 千米	1 - 4 千米
无噪声	0.18	0.68
12 分贝	0.87	1.44
6 分贝	1.83	2.38

C. SWellEx-96 experimental data

C. SWellEx - 96 实验数据

SWellEx-96 data are recorded by the VLA at a sampling rate of 1500 Hz . Due to data corruption, the data from the 22nd hydrophone are excluded from the analysis. Global positioning system (GPS) data from the tow ship and the VLA are used to estimate ranges and synchronize the corresponding time. We analyze data recorded at 23:50-00:06 UTC, which corresponds to distances of 3.7-1.3 km from the VLA. Note that the ship was moving closer to the VLA during this period.

SWellEx - 96 数据由甚大阵 (VLA) 以 1500 Hz 的采样率记录。由于数据损坏，来自第 22 个水听器的数据被排除在分析之外。拖船和 VLA 的全球定位系统 (GPS) 数据用于估计距离并同步相应时间。我们分析了协调世界时 (UTC)23:50 - 00:06 记录的数据，这对应于距 VLA 3.7 - 1.3 千米的距离。请注意，在此期间船正在靠近 VLA。

The signal is divided into 817 snapshots, each 2.73 s $\left(2^{12}\right.$ samples) long, with a 50% overlap. These snapshots are then analyzed using a fast Fourier transform (FFT). Due to the towed source in the SWellEx-96

experiment, the measurements were affected by the Doppler shift. [43,52] To account for Doppler offset, we select the FFT bin with the maximum power within the range of 109 ± 0.5 Hz .

信号被分为 817 个快照，每个快照长 2.73 秒 ($(2^{12}$ 个样本)，重叠率为 50%。然后使用快速傅里叶变换 (FFT) 对这些快照进行分析。由于 SWellEx - 96 实验中的拖曳源，测量受到多普勒频移的影响。[43,52] 为了考虑多普勒偏移，我们在 109 ± 0.5 Hz 范围内选择功率最大的 FFT 频段。

From the entire processed data, a specific subset is selected for the training dataset, which follows the source-receiver configuration depicted in Fig. 6(a), consistent with the simulation analysis. The only difference lies in the number of range samples N_r . For range samples, the training dataset encompasses snapshots from 3.5 km (61st snapshot) to 1.5 km (736th snapshot) relative to the VLA but excludes data from the ranges of $2.1-2.3$ km and $2.7-2.9$ km , yielding a total of $N_r = 537$ samples. For receiver configuration, the training dataset consistently utilizes a uniformly spaced subset of 13 elements (elements 1-61).

从整个处理后的数据中，为训练数据集选择了一个特定子集，该子集遵循图 6(a) 所示的源 - 接收器配置，与模拟分析一致。唯一的区别在于距离样本的数量 N_r 。对于距离样本，训练数据集包括相对于 VLA 从 3.5 千米 (第 61 个快照) 到 1.5 km (第 736 个快照) 的快照，但不包括 $2.1-2.3$ km 和 $2.7-2.9$ km 范围内的数据，总共产生 $N_r = 537$ 个样本。对于接收器配置，训练数据集始终使用 13 个均匀间隔元素 (元素 1 - 61) 的子集。

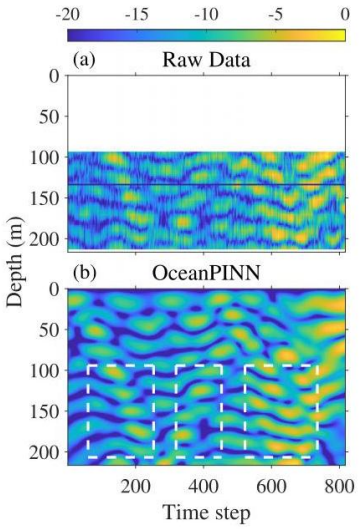

FIG. 8. (Color online) Normalized sound pressure level (dB) of (a) raw data, (b) OceanPINN predicted data with the boundaries of measurements indicated (white boxes).

图 8.(彩色在线)(a) 原始数据、(b)OceanPINN 预测数据的归一化声压级 (dB)，测量边界已标明 (白色方框)。

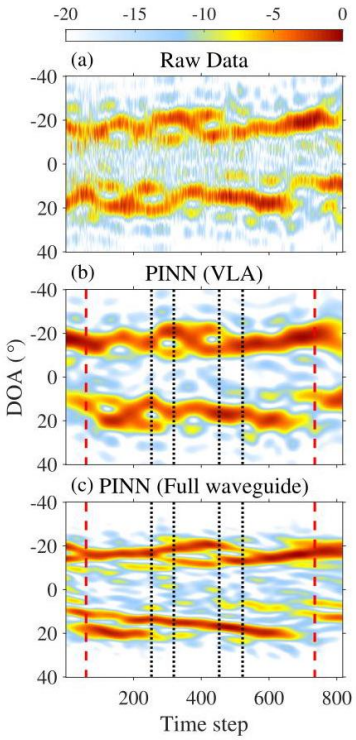

FIG. 9. (Color online) Conventional beamforming (dB) from (a) raw data, (b) OceanPINN predictions within VLA depth, (c) across the full water column. The measurement boundaries are at 1.5 and 3.5 km (black dashed), while the excluded sections are at $2.1-2.3$ and $2.7-2.9$ km (red dotted).

图 9.(彩色在线)(a) 原始数据、(b)VLA 深度内 OceanPINN 预测、(c) 整个水柱的传统波束形成 (dB)。测量边界在 1,5 和 3.5 km 处 (黑色虚线)，而排除部分在 $2.1-2.3$ 和 $2.7-2.9$ km 处 (红色虚线)。

D. SWellEx-96 experimental results

D. SWellEx - 96 实验结果

OceanPINN is trained over 1200000 epochs. Once OceanPINN is trained, the pressure field is generated on a uniform (r, z) grid. Here, r corresponds to the range of each snapshot, and z consists of 300 uniformly distributed points spanning the full water column $0-216.5$ m .

OceanPINN 经过超过 1200000 个轮次的训练。一旦 OceanPINN 训练完成，压力场在均匀的 (r, z) 网格上生成。这里，r 对应每个快照的距离范围，z 由跨越整个水柱 $0-216.5$ m 的 300 个均匀分布点组成。

Figure 8 illustrates the normalized SPLs of the raw data and the OceanPINN prediction, normalized with respect to the maximum of the raw data. The data from the 22nd element [black line in Fig. 8(a)] is excluded from the analysis due to corruption. The SPL increases over time since the source approaches. Comparisons are confined to the VLA region due to no measurements above it. The OceanPINN predictions show a good agreement with the experimental data within the interpolated range $(1.5-3.5$ km) , including the excluded

parts not used for training. Nevertheless, discrepancies are noted in some parts of the extrapolated range. Additionally, the OceanPINN-predicted pressure field exhibits reduced noise features compared to the raw data.

图 8 展示了原始数据和 OceanPINN 预测的归一化声压级 (SPL)，相对于原始数据的最大值进行了归一化。由于损坏，来自第 22 个元素的数据 [图 8(a) 中的黑线] 被排除在分析之外。随着源靠近，声压级随时间增加。由于上方没有测量数据，比较仅限于 VLA 区域。OceanPINN 预测在插值范围 (1.5 − 3.5 km) 内与实验数据显示出良好的一致性，包括未用于训练的排除部分。然而，在外推范围内的某些部分存在差异。此外，与原始数据相比，OceanPINN 预测的压力场具有降低的噪声特征。

We validate the physical consistency of OceanPINN predictions by comparing their DOA using conventional beamforming. This comparison allows us to indirectly validate the predictions in unmeasured regions above the VLA. The beamforming is normalized by the maximum value. Figure 9 shows the beamforming from raw data, OceanPINN prediction within VLA depth, and OceanPINN prediction for the whole water column. The DOA from OceanPINN prediction shows good agreement with raw data. Similar to the magnitude, the interpolated range (1.5 − 3.5 km) showed consistency, while the extrapolated range showed slight differences. Since the array aperture length is identical in Figs. 9(a) and 9(b), beamforming results show the same resolution. While Fig. 9(c) uses an extended array, it shows improved angular resolution, and can distinguish multipath. The results indicate that the OceanPINN prediction is consistent physically. Moreover, akin to Fig. 8, the noisy feature is decreased in the beam-formings from OceanPINN predictions.

我们通过使用传统波束形成比较海洋 PINN 预测的波达方向 (DOA) 来验证其物理一致性。这种比较使我们能够间接验证甚大阵 (VLA) 上方未测量区域的预测。波束形成通过最大值进行归一化。图 9 展示了来自原始数据的波束形成、VLA 深度内的海洋 PINN 预测以及整个水柱的海洋 PINN 预测。海洋 PINN 预测的 DOA 与原始数据显示出良好的一致性。与幅度类似，插值范围 (1.5 − 3.5 km) 显示出一致性，而外推范围则显示出轻微差异。由于图 9(a) 和 9(b) 中的阵列孔径长度相同，波束形成结果显示出相同的分辨率。虽然图 9(c) 使用了扩展阵列，但它显示出改进的角分辨率，并且能够区分多径。结果表明海洋 PINN 预测在物理上是一致的。此外，与图 8 类似，海洋 PINN 预测的波束形成中的噪声特征有所降低。

V. CONCLUSION

五、结论

We introduced an approach named OceanPINN, which uses the PINN for predicting acoustic pressure fields in ocean waveguides from partially measured data. OceanPINN can be considered a method that performs interpolation and extrapolation from a few sampled points based on physics knowledge. Specifically, the neural network is trained with a physics-based loss that enforces the governing equation and the surface-boundary condition.

我们引入了一种名为 OceanPINN 的方法，该方法使用物理信息神经网络 (PINN) 从部分测量数据预测海浪波导中的声压场。OceanPINN 可以被认为是一种基于物理知识从少数采样点进行插值和外推的方法。具体来说，神经网络通过基于物理的损失函数进行训练，该损失函数强制执行控制方程和表面边界条件。

The rapid phase variations of the complex pressure field in the ocean acoustic environment pose two challenges for applying the PINN framework. The first is spectral bias, which we mitigated by transforming the high-wavenumber pressure field into a low-wavenumber envelope. The second is the inaccuracy of phase measurements; we addressed this by training solely on the magnitude of the measured pressure data.

海洋声学环境中复压力场的快速相位变化对应用 PINN 框架提出了两个挑战。第一个是频谱偏差，我们通过将高波数压力场转换为低波数包络来减轻这种偏差。第二个是相位测量的不准确性；我们通过仅对测量压力数据的幅度进行训练来解决这个问题。

The simulations indicated that OceanPINN can accurately predict unmeasured pressure fields. Moreover, results show that OceanPINN can infer phase information solely from magnitude data. In real data applications, OceanPINN predictions match well with VLA measurements and show physically consistent predictions, even above the VLA, which is unmeasured in the experiment. However, the performance of OceanPINN degrades in the extrapolated range, both in simulations and experimental data, which is possibly an inherent weakness of PINNs.

模拟结果表明，OceanPINN 能够准确预测未测量的压力场。此外，结果显示 OceanPINN 仅从幅度数据就能推断出相位信息。在实际数据应用中，OceanPINN 的预测与甚大阵 (VLA) 测量结果匹配良好，并且显示出物理上一致的预测，甚至在实验中未测量的甚大阵之上也是如此。然而，在模拟和实验数据中，OceanPINN 在推断范围内的性能都会下降，这可能是物理信息神经网络 (PINNs) 的一个固有弱点。

ACKNOWLEDGMENTS

致谢

This research was supported by the Korea Institute for Advancement of Technology (KIAT) grant funded by the Korea Government (MOTIE) (Grant No. P0017304, Human Resource Development Program for Industrial Innovation), and the National Research Foundation of Korea (NRF) grant funded by the Korea government (MSIT) (Grant No. 2021R1F1A1045480), and the Office of Naval Research, Grant No. N00014-21-1-2267.

本研究得到了由韩国政府 (贸易、工业和能源部) 资助的韩国产业技术振兴院 (KIAT) 项目 (项目编号:P0017304，产业创新人力资源开发项目)、韩国政府 (科学和信息通信技术部) 资助的韩国国家研究基金会 (NRF) 项目 (项目编号:2021R1F1A1045480) 以及美国海军研究办公室项目 (项目编号:N00014-21-1-2267) 的支持。

AUTHOR DECLARATIONS Conflict of Interest

作者声明利益冲突

The authors have no conflicts to disclose.

作者没有利益冲突需要披露。

DATA AVAILABILITY

数据可用性

The data that support the findings of this study are available from the corresponding author upon reasonable request.

支持本研究结果的数据可在合理要求下从相应作者处获得。

APPENDIX A: COLLOCATION POINT SAMPLING

附录 A: 搭配点抽样

Within the PINN framework, the correct solution is known only at a few points. The values at the remaining unknown points are deduced by minimizing the PDE residual defined as

在 PINN 框架内，仅在少数点上知道正确解。其余未知点的值通过最小化定义为的 PDE 残差来推导

$$\mathcal{R}(\theta) = \mathcal{N}[\hat{u}(x;\theta)] - f(x) \tag{A1}$$

in the general PINN framework in Sec. II C. However, it is important to note that a small PDE residual does not necessarily imply a correct solution. For instance, in our problem, a trivial solution of $\psi(r,z) = 0$ also effectively minimizes the PDE residual. According to Ref. 51, for training PINNs to converge correctly, the correct solution needs to propagate from known points to unknown points throughout iterations. Failure in this propagation can lead subsequent points to convergence to the trivial solution. The PDE residual calculated at a specific collocation point is influenced only by nearby values, and if these nearby values are incorrect, that local region can exhibit a low PDE residual even if it is not a correct solution. Such a failure in propagation is also observed in OceanPINN. As seen in Fig. 7(d), in a far extrapolated range near 4 km , the predicted pressure field shows a trivial solution of $p(r,z) = 0$ in several areas.

然而，在第二节 C 部分的一般 PINN 框架中。需要注意的是，小的偏微分方程残差并不一定意味着解是正确的。例如，在我们的问题中，$\psi(r,z) = 0$ 的平凡解也能有效地使偏微分方程残差最小化。根据参考文献 51，为了训练 PINN 正确收敛，在整个迭代过程中，正确的解需要从已知点传播到未知点。这种传播失败会导致后续点收敛到平凡解。在特定配置点计算的偏微分方程残差仅受附近值的影响，如果这些附近值不正确，即使该局部区域不是正确解，它也可能表现出低偏微分方程残差。在 OceanPINN 中也观察到了这种传播失败。如图 7(d) 所示，在 4 km 附近的远外推范围内，预测的压力场在几个区域显示出 $p(r,z) = 0$ 的平凡解。

As training progresses, PINN can be converged to solutions that have two distinct regions: one region converges to the correct solutions, while the other converges to trivial solutions. Although both regions show low PDE residuals, the narrow boundary between them is likely to exhibit high PDE residuals. However, since PDE loss is averaged over all collocation points, the loss remains small, if collocation points are uniformly distributed and most areas show low PDE residuals. This can lead to challenges in updating and getting stuck in local minima. We adopt Retain-Resample-Release (R3) sampling, [51] which accumulates collocation points

in high PDE residual regions to address this problem. Specifically, R3 sampling determines collocation points by retaining half of the points with high PDE residuals from the previous iteration and resampling the other half from a uniform random distribution.

随着训练的进行，PINN 可以收敛到具有两个不同区域的解: 一个区域收敛到正确解，而另一个区域收敛到平凡解。尽管两个区域的偏微分方程 (PDE) 残差都很低，但它们之间的狭窄边界可能会表现出高 PDE 残差。然而，由于 PDE 损失是在所有配置点上平均的，如果配置点均匀分布且大多数区域显示低 PDE 残差，损失仍然很小。这可能会导致更新过程中的挑战并陷入局部最小值。我们采用保留 - 重采样 - 释放 (R3) 采样，[51] 它在高 PDE 残差区域累积配置点以解决此问题。具体而言，R3 采样通过保留上一次迭代中具有高 PDE 残差的一半点并从均匀随机分布中对另一半进行重采样来确定配置点。

As OceanPINN has a real and imaginary output, during a training process, the real (R_r) and imaginary (R_i) PDE residuals are computed separately for collocation point $\left\{r_n^i, z_n^i\right\}_{i=1}^{N_n}$, and summed for calculating PDE loss $\mathcal{L}_\mathcal{N}$ as

由于 OceanPINN 有实部和虚部输出，在训练过程中，针对配置点 $\left\{r_n^i, z_n^i\right\}_{i=1}^{N_n}$ 分别计算实部 (R_r) 和虚部 (R_i) 的 PDE 残差，并将它们相加用于计算 PDE 损失 $\mathcal{L}_\mathcal{N}$，如下所示

$$\mathcal{L}_\mathcal{N}(\theta) = \frac{1}{N_n}\sum_{k=1}^{N_n}\left|R_\mathrm{r}^k(\theta) + iR_\mathrm{i}^k(\theta)\right|^2, \tag{A2}$$

$$R_\mathrm{r}^k(\theta) = \frac{\partial^2\widehat{\psi}_\mathrm{r}^k}{\partial r^2} + 2k_0\frac{\partial\widehat{\psi}_\mathrm{i}^k}{\partial r} + \frac{\partial^2\widehat{\psi}_\mathrm{r}^k}{\partial z^2} + k_0^2\left(n^2-1\right)\widehat{\psi}_\mathrm{r}^k, \tag{A3}$$

$$R_\mathrm{i}^k(\theta) = \frac{\partial^2\widehat{\psi}_\mathrm{i}^k}{\partial r^2} - 2k_0\frac{\partial\widehat{\psi}_\mathrm{r}^k}{\partial r} + \frac{\partial^2\widehat{\psi}_\mathrm{i}^k}{\partial z^2} + k_0^2\left(n^2-1\right)\widehat{\psi}_\mathrm{i}^k, \tag{A4}$$

where superscript k denotes corresponding to the k th collocation point.

其中上标 k 表示对应于第 k 个配置点。

We aim to accumulate collocation points with either high real or imaginary PDE residuals to achieve a balance between the real and imaginary residuals of the PDE. The pseudo-code of the sampling method for collocation points is described in Algorithm I.

我们旨在累积具有高实部或虚部 PDE 残差的配置点，以实现 PDE 实部和虚部残差之间的平衡。配置点采样方法的伪代码在算法 I 中描述。

APPENDIX B: LOSS WEIGHT COEFFICIENTS

附录 B: 损失权重系数

PINNs utilize a composite loss function comprising physics-based loss and data-fitting terms. The general form of the PINN composite loss function can be represented as

PINN 使用由基于物理的损失和数据拟合项组成的复合损失函数。PINN 复合损失函数的一般形式可以表示为

$$\mathcal{L}(\theta) = \sum_{i=1}^{M} \lambda_i \mathcal{L}_i(\theta). \tag{B1}$$

With this loss function, neural network parameters θ are typically updated with the gradient descent as [60]

使用此损失函数，神经网络参数 θ 通常通过梯度下降更新为 [60]

$$\theta_{n+1} = \theta_n - \eta \sum_{i=1}^{M} \lambda_i \nabla_\theta \mathcal{L}_i(\theta_n), \tag{B2}$$

where η denotes the learning rate. Disparities in the gradients of these loss terms can lead to discrepancies in the convergence rates of each component. Disparities in the gradients of each loss term $\nabla_\theta \mathcal{L}_i(\theta_n)$ can lead to discrepancies in the convergence rates of each component. [36,60] Loss weight coefficients address this issue, as they rescale the learning rate of each loss term $\mathcal{L}_i$ to $\eta\lambda_i$ and balance the convergence rate across different loss terms.

其中 η 表示学习率。这些损失项梯度的差异可能导致每个组件收敛速度的差异。每个损失项 $\nabla_\theta \mathcal{L}_i(\theta_n)$ 的梯度差异可能导致每个组件收敛速度的差异。[36,60] 损失权重系数解决了这个问题，因为它们将每个损失项 $\mathcal{L}_i$ 的学习率重新调整为 $\eta\lambda_i$，并平衡不同损失项之间的收敛速度。

OceanPINN utilizes three loss terms: $\mathcal{L}_\mathcal{N}$ ensures adherence to the governing equation, while $\mathcal{L}_\mathcal{M}$ and $\mathcal{L}_\mathcal{B}$ adjust the OceanPINN prediction at sampling points to match measured and surface pressures. The formulation of $\mathcal{L}_\mathcal{N}$ deviates from the other two, potentially leading to discrepancies in gradient magnitudes. Considering these distinctions, we test various loss weight coefficients of $\lambda_N = \left\{10^2, 10^3, 10^4, 10^5, 10^6\right\}$, while setting $\lambda_M = \lambda_B = 1$. The best results are obtained from $\lambda_N = 10^5$ for every SWellEx-96 simulation in Sec. IV A, as shown in Fig. 10. $\lambda_N = 10^4$ also demonstrates predictions close to the true solution and $\lambda_N = 10^3$ yields favorable results in the noiseless scenario.

OceanPINN 使用三个损失项: $\mathcal{L}_\mathcal{N}$ 确保符合控制方程，而 $\mathcal{L}_\mathcal{M}$ 和 $\mathcal{L}_\mathcal{B}$ 在采样点调整 OceanPINN 预测以匹配测量压力和表面压力。$\mathcal{L}_\mathcal{N}$ 的公式与其他两个不同，可能导致梯度大小的差异。考虑到这些差异，我们测试了 $\lambda_N = \left\{10^2 、 10^3, 10^4, 10^5, 10^6\right\}$ 的各种损失权重系数，同时设置 $\lambda_M = \lambda_B = 1$。如第 IV A 节中每个 SWellEx - 96 模拟的图 10 所示，从 $\lambda_N = 10^5$ 获得了最佳结果。$\lambda_N = 10^4$ 也展示了接近真实解的预测，并且 $\lambda_N = 10^3$ 在无噪声场景中产生了良好的结果。

ALGORITHM 1. Retain-Resample-Release (R3) sampling algorithm for OceanPINN.

算法 1. OceanPINN 的保留 - 重采样 - 释放 (R3) 采样算法。

1: Sample the initial population $\mathcal{P}_0$ of collocation points $\left\{x_n^i\right\}_{i=1}^{N_n}$ from a uni-

1: 从均匀分布 $\mathcal{P}_0$ 中采样初始配置点种群 $\mathcal{P}_0$ $\{x_n^i\}_{i=1}^{N_n}$

form distribution $U(\Omega)$

均匀分布 $U(\Omega)$

for $i = 0$ to max. iteration -1 do

for $i = 0$ 到最大迭代次数 - 1 执行

Compute the real (R_r) and imaginary (R_i) PDE residuals of collocation

计算配置点处的实 (R_r) 和虚 (R_i) 偏微分方程残差

points $x_n \in \mathcal{P}_i$

点 $x_n \in \mathcal{P}_i$

Sort R_r and R_i

对 R_r 和 R_i 进行排序

Select populations $\mathcal{P}_{i,\,\mathrm{real}}^{\mathrm{r}}$ and $\mathcal{P}_{i,\,\mathrm{imag}}^{\mathrm{r}}$ such that satisfy top one-third R_r

选择满足前三分一 R_r 的总体 $\mathcal{P}_{i,\,\mathrm{real}}^{\mathrm{r}}$ 和 $\mathcal{P}_{i,\,\mathrm{imag}}^{\mathrm{r}}$

and R_i

以及 R_i

Merge two populations except overlapping $\mathcal{P}_i^{\mathrm{r}} \leftarrow \mathcal{P}_{i,\,\mathrm{real}}^{\mathrm{r}} \cup \mathcal{P}_{i,\,\mathrm{imag}}^{\mathrm{r}}$

合并两个总体，但不包括重叠的 $\mathcal{P}_i^{\mathrm{r}} \leftarrow \mathcal{P}_{i,\,\mathrm{real}}^{\mathrm{r}} \cup \mathcal{P}_{i,\,\mathrm{imag}}^{\mathrm{r}}$

Retain $\mathcal{P}_i^{\mathrm{r}}$ and resample the population $\mathcal{P}_i^{\mathrm{s}}$ from a uniform distribution

保留 $\mathcal{P}_i^{\mathrm{r}}$ 并从均匀分布中对总体 $\mathcal{P}_i^{\mathrm{s}}$ 进行重采样

$U(\Omega)$
Merge the two population $\mathcal{P}_{i+1} \leftarrow \mathcal{P}_i^{\mathrm{r}} \cup \mathcal{P}_i^{\mathrm{s}}$

合并两个总体 $\mathcal{P}_{i+1} \leftarrow \mathcal{P}_i^{\mathrm{r}} \cup \mathcal{P}_i^{\mathrm{s}}$

end for

结束循环

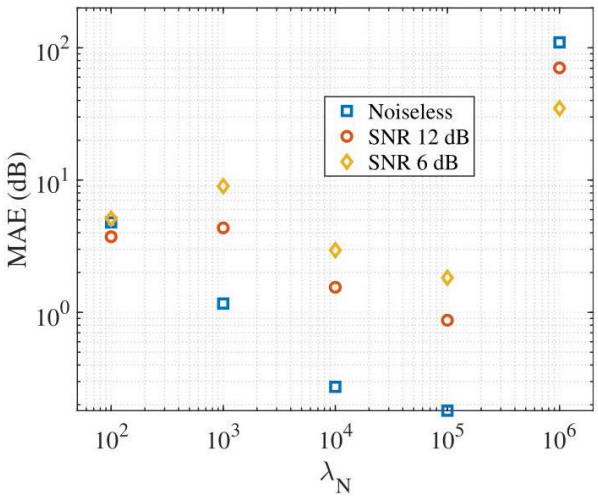

FIG. 10. (Color online) MAE (dB) of the OceanPINN predicted field's sound pressure level, trained with different λ_N and SWellEx-96 simulation data with different SNRs from Sec. IV A.

图 10.(在线彩色) 使用不同的 λ_N 和来自第四节 A 部分的具有不同信噪比的 SWellEx - 96 模拟数据训练的 OceanPINN 预测场的声压级的平均绝对误差 (dB)。

Figure 11 shows examples of predictive failure in the noiseless SWellEx-96 simulation scenario due to inappropriate λ_N values. As shown in Fig. 11(a), relatively low values of λ_N can lead OceanPINN to overfit at measured and surface points. In contrast, as depicted in Fig. 11(b), an overly high λ_N can lead OceanPINN to converge to trivial solutions, i.e., zero pressure field. This trivial solution satisfies the homogeneous Helmholtz equation, and can easily reduce $\mathcal{L}_{\mathcal{N}}$, though not a meaningful solution. MAE in Fig. 10 is high for $\lambda_N = 10^6$ due to the pressure being close to zero.

图 11 展示了在无噪声的 SWellEx - 96 模拟场景中由于 λ_N 值不合适导致的预测失败示例。如图 11(a) 所示，相对较低的 λ_N 值会导致 OceanPINN 在测量点和表面点处出现过拟合。相反，如图 11(b) 所示，过高的 λ_N 会导致 OceanPINN 收敛到平凡解，即零压力场。这个平凡解满足齐次亥姆霍兹方程，并且可以轻松降低 $\mathcal{L}_{\mathcal{N}}$ ，尽管不是一个有意义的解。由于压力接近零，图 10 中 $\lambda_N = 10^6$ 的平均绝对误差较高。

At low SNR, the MAE increases with lower λ_N . This is attributed to a lower λ_N amplifying the impact of the reconstruction loss, which leads to overfitting to noisy measured data. However, a lower λ_N facilitates faster model

在低信噪比下，平均绝对误差随着 λ_N 的降低而增加。这归因于较低的 λ_N 放大了重建损失的影响，从而导致对有噪声的测量数据过拟合。然而，较低的 λ_N 有助于模型更快地

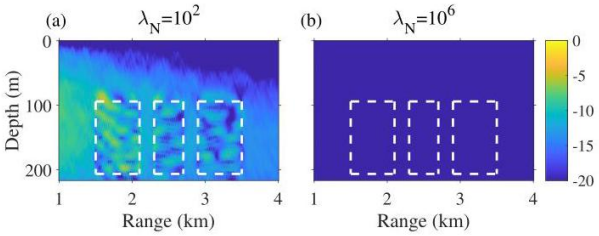

FIG. 11. (Color online) The normalized sound pressure level (dB) of OceanPINN predicted pressure field, which is trained with (a) $\lambda_N = 10^2$,(b) $\lambda_N = 10^6$.

图 11.(在线彩色) 使用 (a) $\lambda_N = 10^2$ 、(b) $\lambda_N = 10^6$ 训练的 OceanPINN 预测压力场的归一化声压级 (dB)。